Parametric effects of fiber nonlinearity impairment in WDM-based PON networks

YAN XU[1], ASAD SALEEM[2], ZHEN LI[1,*], SHUAI WANG[1,*]
[1]*Zaozhuang University, School of Opto-Electronic Engineering, Zaozhuang 277100, China*
[2]*Zhejiang University-University of Illinois Urbana-Champaign Institute (ZJU-UIUC), Hangzhou 314400, China*

In recent years, with the rise of the emerging services such as 4K or 8K ultra-high-definition television, high-definition video games, cloud computing, etc., the users' demands for bandwidth have continued to increase. In order to solve this problem, the wavelength division multiplexing (WDM) based passive optical network (PON) is employed. However, when multiple wavelengths are transmitted simultaneously in the optical fiber, fiber nonlinearity issues would occur, reducing the system's capacity and transmission range. In this paper, different parametric effects on the fiber nonlinearity impairments, including four-wave mixing (FWM), cross-phase modulation (XPM), and stimulated Raman scattering (SRS), are adequately investigated by theoretical analysis and simulations. In addition, the fiber nonlinearity impairments induced sensitivity penalty and optical power changes in WDM-based PON are discussed in detail. Given that the constructed simulation systems incorporate modular design, advanced WDM techniques, and ensure compatibility and interoperability for upcoming network technologies and escalating bandwidth requirements, the results yielded offer in-depth insights into the nonlinear effects within WDM-based PON networks, along with comprehensive details for developing WDM-based PON networks of enhanced performance.

(Received October 30, 2023; accepted June 5, 2024)

Keywords: Wavelength division multiplexing, Passive optical network, Four-wave mixing, Cross-phase modulation, Stimulated Raman scattering

1. Introduction

Over the past two decades, the demands for Internet bandwidth have increased dramatically, driving a steady increase in global Internet traffic. According to the Cisco Global Visual Networking Index, the global IP traffic is expanding at a compound annual growth rate (CAGR) of 26% from 2017-2022 [1, 2]. In the meantime, the impact of COVID-19 has necessitated a shift for many from offline to online work and lifestyle modalities, including telework, distance learning, entertainment, and instant messaging through the internet [3, 4]. This transition has introduced additional demands on the existing network capacity. Currently, the optical access network (OAN) is conceived as an important tool for accelerating Internet transmission speed. The time division multiplexing (TDM)-based optical access network (PON), which is the industry standard in PON technology, is evidently unable to keep up with the population's growing demand for bandwidth as it will be constrained by the bandwidth of device [4]. Wavelength division multiplexing (WDM) technology is a widely adopted method for enhancing the total capacity of optical transmission networks, offering advantages such as substantial transmission capacity, extended transmission range, protocol transparency, and straightforward management and upgrading [5]. However, when multiple wavelengths are transmitted simultaneously in the optical fiber, the nonlinearity impairment would drastically lower the transmission capacity and range.

In WDM-based PON networks, in addition to the challenges from polarization mode dispersion and nonlinear dispersion variations [6], which any transmission system will face if a fiber is used as the transmission channel, the main nonlinear impairments are caused by four-wave mixing (FWM), cross-phase modulation (XPM), and stimulated Raman scattering (SRS). So far, numerous studies on the aforementioned nonlinear impairments have been carried out in literature [7, 8]. For the investigation of FWM nonlinear impairment, X. Miao et al. studied the effect of chirped directly modulated laser (DML) on the FWM nonlinear impairment in a multi-wavelength NG-EPON system [9]. X. Wu et al. simulated the FWM nonlinear impairment in next generation Ethernet PON (NG-EPON) system and proposed a candidate wavelength scheme for future NG-EPON [10]. Y. Song et al. investigated the FWM nonlinear impairment effects on the bit error rate (BER) in the 5G fronthaul OAN through experiment [5]. For the study of XPM nonlinear impairment, R. Oliveira et al. experimentally investigated the XPM nonlinear impairment in time and wavelength division multiplexed PON (TWDM-PON) [11]. M. Abdulnabi et al. simulated the XPM and FWM nonlinear impairments in next generation PON stage-2 (NG-PON2) system [12]. R. Pagare et al. studied various nonlinear impairments (including the XPM nonlinear impairment) in NG-PON2 system based on TWDM-PON architecture [13]. For the study of SRS nonlinear impairment, R. Gaudino et al. analyzed the SRS nonlinear impairment when multiple PON protocols are coexisting [14]. V. Curri et al. provided

a compact theoretical framework to investigate the SRS-induced attenuation due to the coexistence of TWDM-PON and GPON [15]. G. Simon et al. investigated the power penalty resulting from SRS nonlinear degradation in the presence of NG-PON2 and GPON [16]. However, research into how various factors (such as bit rate, channel spacing, chromatic dispersion, fiber length, input power, number of channels, dispersion slope, chirp coefficient, fiber attenuation, insertion loss, and dark current) influence the specified fiber nonlinearity impairments within WDM-based PON networks has been limited, indicating a need for further investigation.

In this paper, we investigate different parameters effect on the FWM, XPM, and SRS nonlinearity impairments in WDM-based PON networks, including the bit rate, channel spacing, chromatic dispersion, fiber length, input power, number of channels, dark current, insertion loss, dispersion slope, fiber attenuation and chirp coefficient. Furthermore, the sensitivity penalty and optical power changes caused by the fiber nonlinearity impairments are provided under the condition of different parameters. Theoretical discussion and simulation results of the above-mentioned fiber nonlinearity impairments can be found in the following sections.

2 Theoretical analysis of the fiber nonlinearity impairments

2.1. Theoretical analysis of the FWM nonlinearity impairment

The FWM nonlinearity impairment occurs when two or three wavelengths are simultaneously transmitted through the optical fiber, leading to the generation of new wavelengths as a result of FWM nonlinearity. Should these newly generated wavelengths overlap with the transmitted wavelength band, crosstalk will ensue. Furthermore, FWM nonlinearity can also result in power attenuation of the transmitted wavelengths [17]. When N wavelengths are transmitted simultaneously in the optical fiber, M new wavelengths will be generated due to the existence of the FWM nonlinearity impairment. The newly generated wavelength M can be expressed as

$$M = \frac{N^2}{2}\left(N-1\right) \tag{1}$$

It is concluded that, M will increase sharply with the increase of the number of transmitted wavelengths. When the generated wavelengths fall into the transmission channels, they will seriously affect the transmission quality of the WDM-based PON networks.

In order to further investigate the FWM nonlinearity impairment, it is assumed that three incident wavelengths (f_i, f_j, and f_k) are transmitted simultaneously in the optical fiber and the generated frequency f_{ijk} can be expressed as follows [18]

$$f_{ijk} = f_i + f_j - f_k \qquad i,j \neq k \tag{2}$$

Then, the output power of f_{ijk} can be described as

$$P_{ijk} = \frac{1024\pi^6}{n^4\lambda^2c^2}(DX)^2\frac{P_iP_jP_k}{{A_{eff}}^2}e^{-\alpha L}\frac{\left(1-e^{-\alpha L}\right)^2}{\alpha^2}\eta \tag{3}$$

with

$$\eta = \frac{\alpha^2}{\alpha^2+\Delta\beta^2}\left[1+\frac{4e^{-\alpha L}sin^2(\Delta\beta L/2)}{\left(1-e^{-\alpha L}\right)^2}\right] \tag{4}$$

and

$$\Delta\beta = -\frac{\lambda^4\pi}{c^2}\frac{dD_c}{d\lambda}\{(f_i-f_0)+(f_j-f_0)\}(f_j-f_k)(f_i-f_k) \tag{5}$$

where n refers the fiber refractive index, λ denotes the transmission wavelength, c is the light speed in vacuum, D represents the degeneracy factor, X is the third-order nonlinear polarizability, A_{eff} refers the effective cross-sectional area of the fiber, α denotes the fiber attenuation coefficient, L is the fiber length, P_i, P_j and P_k denote the optical power of the three incident frequencies (f_i, f_j and f_k), η is the FWM efficiency, $\Delta\beta$ refers the phase mismatch factor, f_0 is the zero-dispersion wavelength of the fiber, and $\frac{dD_c}{d\lambda}$ means the dispersion slope.

In conclusion, the FWM nonlinearity impairment has a close relationship with the number of transmitted wavelengths (N), input optical power (P_i, P_j, and P_k), fiber length (L), fiber zero-dispersion wavelength (f_0), channel spacing (f_i - f_k), etc.

2.2. Theoretical analysis of the XPM nonlinearity impairment

The XPM nonlinearity impairment denotes that when two or more incident wavelengths of different frequencies are transmitted simultaneously in the optical fiber, the intensity fluctuation of each incident wavelength can modulate the phase of other incident wavelengths by changing the refractive index of the optical fiber. Here, a system with two channels is installed for analyzing the XPM nonlinearity impairment. We assume that the two incident wavelengths are in the same polarization state and the group velocity dispersion (GVD) only causes the walk-off effect to the optical field $A_j(z,t)$. Then, the wave equation can be written as following [19]

$$\frac{\partial A_j}{\partial z}+\frac{\alpha}{2}A_j+\frac{1}{v_{gj}}\frac{\partial A_j}{\partial t} = i\gamma_j(\left|A_j\right|^2+2|A_k|^2)A_j \tag{6}$$

where v_{gj} is the group velocity, α denotes the fiber attenuation coefficient, γ_j refers the nonlinear coefficient, j, $k = 1$ or 2, $j \neq k$.

The general solution of Eq. (6) can be expressed as follows

$$A_j(z,t) = A_j\left(0,t-z/v_{gj}\right)\exp(-\alpha z/2)\exp(i\emptyset_j(z,t)) \tag{7}$$

with

$$\emptyset_j(z,t) = \gamma_j \begin{bmatrix} \frac{1-e^{-\alpha z}}{\alpha}\left|A_j\left(0, t-\frac{z}{v_{gj}}\right)\right|^2 + \\ 2\int_0^z \left|A_k(0, t-\frac{z}{v_{gj}}+d_{jk}z')\right|^2 e^{-\alpha z'}dz' \end{bmatrix} \quad (8)$$

where d_{jk} denotes the walk-off parameter, $\phi_j(z,t)$ is the phase shift caused by self-phase modulation (SPM) and XPM.

Subsequently, the optical power of Channels 1 and 2 at $z = 0$ is assumed as following

$$P_1(0,t) = |A_1(0,t)|^2 = P_1 \quad (9)$$

$$P_2(0,t) = |A_2(0,t)|^2 = P_2 + P_{2m}\cos(\Omega_m t) \quad (10)$$

Substituting Eqs. (9) and (10) into Eq. (8), $\phi_j(z,t)$ can be expressed as

$$\emptyset_1(L,t) = \gamma_1(P_1 + 2P_2)L_{eff} + \Delta\emptyset\cos(\Omega_m\left(t - \frac{L}{v_{g1}}\right) + \varphi) \quad (11)$$

with

$$\Delta\emptyset = 2\gamma_1 P_{2m}\sqrt{\eta_{XPM}}L_{eff} \quad (12)$$

and

$$\eta_{XPM} = \frac{\alpha^2}{{\Omega_m}^2 d_{12}^2+\alpha^2}\left[1 + \frac{4sin^2(\Omega_m d_{12}L/2)e^{-\alpha L}}{(1-e^{-\alpha L})^2}\right] \quad (13)$$

where η_{XPM} is the XPM efficiency. The mathematical expressions show that the XPM nonlinearity impairment is closely related to the channel spacing (d_{12}), input optical power (P_1 and P_2), transmission distance (L), GVD, modulation rate (Ω_m), etc.

2.3. Theoretical analysis of the SRS nonlinearity impairment

The SRS nonlinearity impairment is basically an inelastic light scattering phenomenon caused by the vibration of molecules or the vibration of lattices in solids. During the Raman scattering, a photon absorbs or releases a portion of energy, thus producing a small portion of the scattered photons with different frequencies, which is generally lower than that of the incident light. In WDM-based PON networks, the Raman scattering between the pump and signal wavelengths can be written as [20]

$$\frac{\partial P_S}{\partial z} + \frac{1}{v_S}\frac{\partial P_S}{\partial t} = (gP_P - \alpha)P_S \quad (14)$$

$$\frac{\partial P_P}{\partial z} + \frac{1}{v_P}\frac{\partial P_P}{\partial t} = (-gP_S - \alpha)P_P \quad (15)$$

where P_s and P_p refer the power of the pump and signal wavelengths, respectively, V_s and V_p denote the group velocity of pump and signal wavelengths, g is the standard Raman gain coefficient divided by the effective area of the fiber, and α is the fiber attenuation. Here, we only consider the power consumption on the pump wavelengths and ignore the nonlinear Raman gain on the signal wavelengths. Meanwhile, the time-dependent terms on the left side of Eq. (14) and (15) are neglected. Then, Eqs. (14) and (15) can be given as

$$\frac{\partial P_S}{\partial z} = -\alpha P_S \quad (16)$$

$$\frac{\partial P_P}{\partial z} = (-gP_S - \alpha)P_P \quad (17)$$

After the above-mentioned analysis, the SRS-induced power depletion ΔP can be written as

$$\Delta P = \sum_{i=1}^{N}(10\log_{10} e)\frac{g_{Ri}}{A_{eff}}P_S L_{eff} \quad (18)$$

It can be seen that the SRS nonlinearity impairment has a close relationship with the number of transmitted wavelengths (N), power of the signal wavelengths (P_s), fiber length (L_{eff}), channel spacing (g_{R_i}), etc.

3. Simulation setup

3.1. Simulation setup for investigating the parameters effect on FWM nonlinearity impairment

In order to investigate the parametric effect on FWM nonlinearity impairment in the WDM-based PON networks, the simulation setup is considered by using the VPI Transmission Maker, which is a well-known tool for optical communication system analysis and enhances the credibility and accuracy of the simulation results in modeling optical communication systems [21, 22]. It's widely recognized that WDM-based PON networks integrate WDM technology from backbone transmission with the PON system employed in the distributed access network proximate to users. In this context, our analysis focused on the FWM effect within the WDM segment [23, 24]. Due to the identical settings for each simulation system with the exception of one parameter, one simulation system is used as an example (see Fig. 1) and the relevant parameters are listed in Table 1. Four lasers operating at 1300.9 nm, 1305.4 nm, 1310 nm, and 1314.6 nm are used as optical carriers on the Tx side, with a channel spacing of 800 GHz. Then, the optical wavelengths are modulated by 10/25 Gb/s non-return-to-zero (NRZ) signals through Mach-Zehnder modulators (MZMs), where the chirp coefficient of the MZMs is 0. Afterwards, each signal is amplified to 8 dBm and multiplexed by the multiplexer (MUX), whose insertion loss is 1.5 dB. The multiplexed signals are injected into 20 km standard single mode fiber (SSMF) for transmission. According to the above-mentioned theoretical analysis, the FWM nonlinearity impairment is closely related to the fiber zero-dispersion wavelength, therefore, 1310 nm (Channel 3) is set as the zero-dispersion wavelength of the fiber for exploring the most severe FWM. Meanwhile, the fiber attenuation and dispersion slope of the SSMF are set as 0.4 dB/km and 0.093 ps/nm^2·km, respectively. After 20

km SSMF transmission, the wavelengths are filtered by the de-multiplexer (DEMUX) with a 1.5-dB insertion loss. Subsequently, each filtered signal is firstly attenuated by variable optical attenuator (VOA) and then captured by avalanche photodiode (APD), whose dark current is 2×10^{-8}A [25]. Finally, the module of "BER Analyzer" is used for measuring the bit error rate (BER).

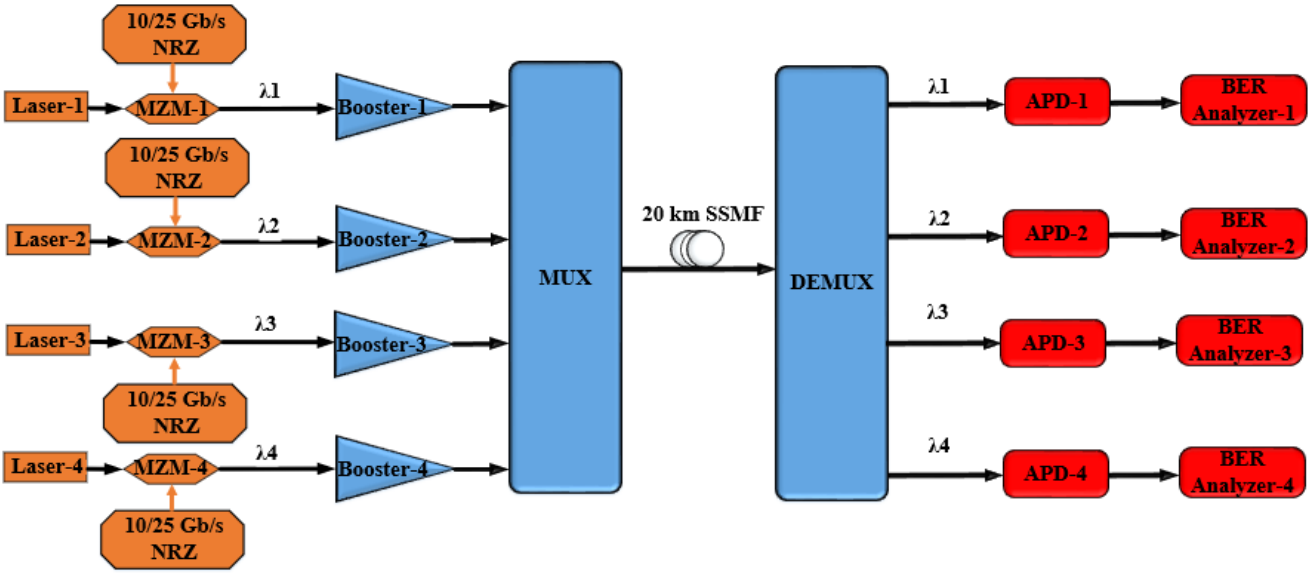

Fig. 1. The simulation setup for measuring the FWM nonlinearity impairment (color online)

Table 1. The adopted parameters in the simulation

Parameters	Value
Number of Channels	4, 8, 12
Channel Spacing	200 GHz, 400 GHz, 800 GHz
Modulation Rate	10 Gb/s, 25 Gb/s
Fiber Attenuation	0.3 dB/km, 0.35 dB/km, 0.4 dB/km
Dispersion Slope	0.073 ps/nm^2·km, 0.083 ps/nm^2·km, 0.093 ps/nm^2·km
Chirp Coefficient	0, 0.5, 1
Out Power	6 dBm, 8 dBm, 10 dBm
Fiber Length	10 km, 20 km, 30 km
MUX/DEMUX Insertion Loss	0.5dB, 1.5 dB, 2.5 dB
Zero-dispersion Wavelength	1310 nm
APD Dark Current	1×10^{-8} A, 1.5×10^{-8} A, 2×10^{-8} A

3.2. Simulation setup for investigating the parameters effect on XPM nonlinearity impairment

Fig. 2 represents the simulation block diagram for investigating the influence of parameters on XPM nonlinearity impairment, and the simulation's input parameters are listed in Table 2. At the transmitter side, 4 wavelengths operating at 1547.9 nm, 1548.7 nm, 1549.5 nm and 1550.3 nm are used as the optical carriers, whereas the channel spacing and electrical signal are set as 100 GHz and 10/25 Gb/s NRZ, respectively. Then, the optical and electrical signals are both injected into the MZMs for modulation, where the chirp coefficient is 0. Afterwards, the modulated signals are amplified to 8 dBm per channel. The four channels are set to the same polarization for the purpose of examining the worst XPM nonlinearity damage. Note that, considering the effects from the random rotation of the polarization states for different wavelengths induced by the SSMF defined by the VPI software, the polarization states of all the channels shall be different during the real simulation. The four channels are multiplexed using MUX with a 1.5 dB insertion loss, and the transmission is done using a 20-km SSMF with a 0.4-dB/km fiber attenuation and a 0.093-ps/nm^2 km dispersion slope. Here, Channel 3 is filtered for BER measurement because Channel 2 or Channel 3 is more affected by XPM nonlinearity impairment than other channels. Subsequently, the filtered signal is captured by APD and finally sent to the "BER Analyzer" module for BER calculation.

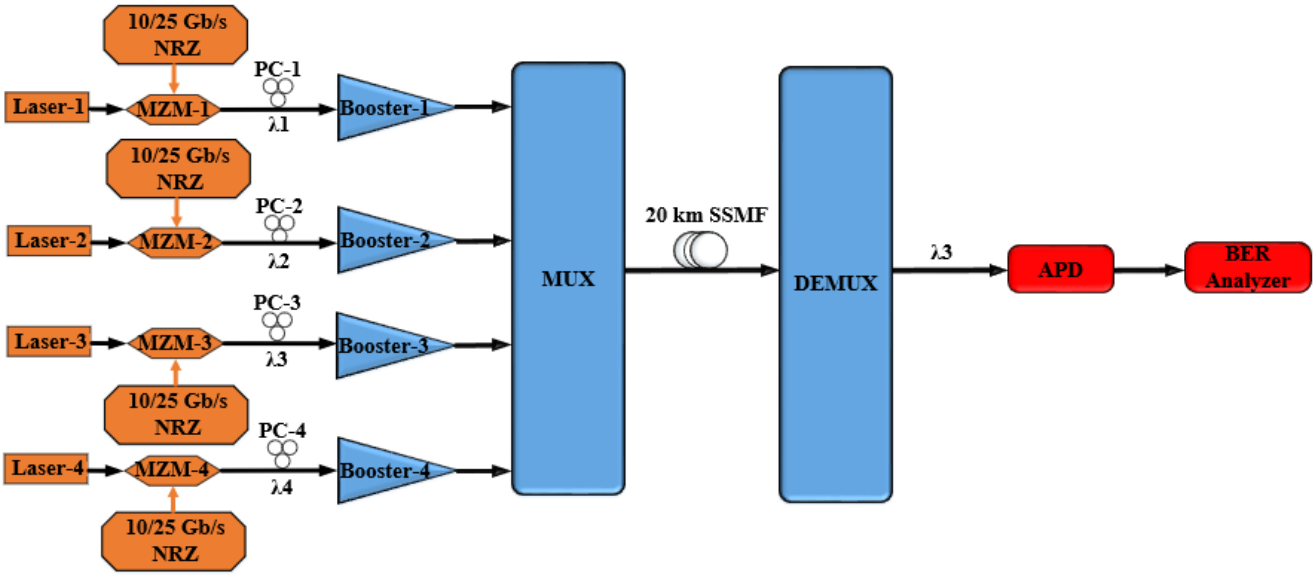

Fig. 2. The simulation setup for investigating the XPM nonlinearity impairment (color online)

Table 2. The employed parameters in the simulation

Parameters	Value
Number of Channels	4, 8, 12
Channel Spacing	50 GHz, 100 GHz, 200 GHz
Modulation Rate	10 Gb/s, 25 Gb/s
Fiber Attenuation	0.15 dB/km, 0.2 dB/km, 0.25 dB/km
Dispersion Slope	0.073 ps/nm^2·km, 0.083 ps/nm^2·km, 0.093 ps/nm^2·km
Chirp Coefficient	0, 0.5, 1
Out Power	6 dBm, 8 dBm, 10 dBm
Fiber Length	10 km, 20 km, 30 km
MUX/DEMUX Insertion Loss	0.5dB, 1.5 dB, 2.5 dB
Dispersion Coefficient	3.5 ps/nm/km, 17 ps/nm/km
APD Dark Current	1×10^{-8} A, 1.5×10^{-8} A, 2×10^{-8} A

3.3. Simulation setup for investigating the parameters effect on SRS nonlinearity impairment

Fig. 3 exhibits the simulation block diagram for studying the parameters affecting the SRS nonlinearity impairment and Table 3 provides the parameters adjustment. At the transmitting ends, 1285 nm, 1289.4 nm, 1293.9 nm, and 1298.4 nm are selected as the optical carriers for the upstream, whereas 1335.2 nm, 1340 nm, 1344.8 nm, and 1349.7 nm are used for the downstream. Then, MZMs are utilized for modulating 10/25 Gb/s NRZ signals on the upstream and downstream wavelengths. The output power of both upstream and downstream is 8 dBm per channel. After amplification, upstream and downstream signals are sent to the MUXs, whose insertion loss is 1.5 dB. Afterwards, making use of 20 km SSMF for bi-direction transmission, where the zero-dispersion wavelength is 1310 nm (the FWM nonlinearity impairment can be ignored), the fiber attenuation is 0.4 dB/km and the dispersion slope is 0.093 ps/nm^2·km. Eventually, for measuring the SRS-induced optical power changes, "Signal Analyzer" modules are used before and after the SSMF transmission.

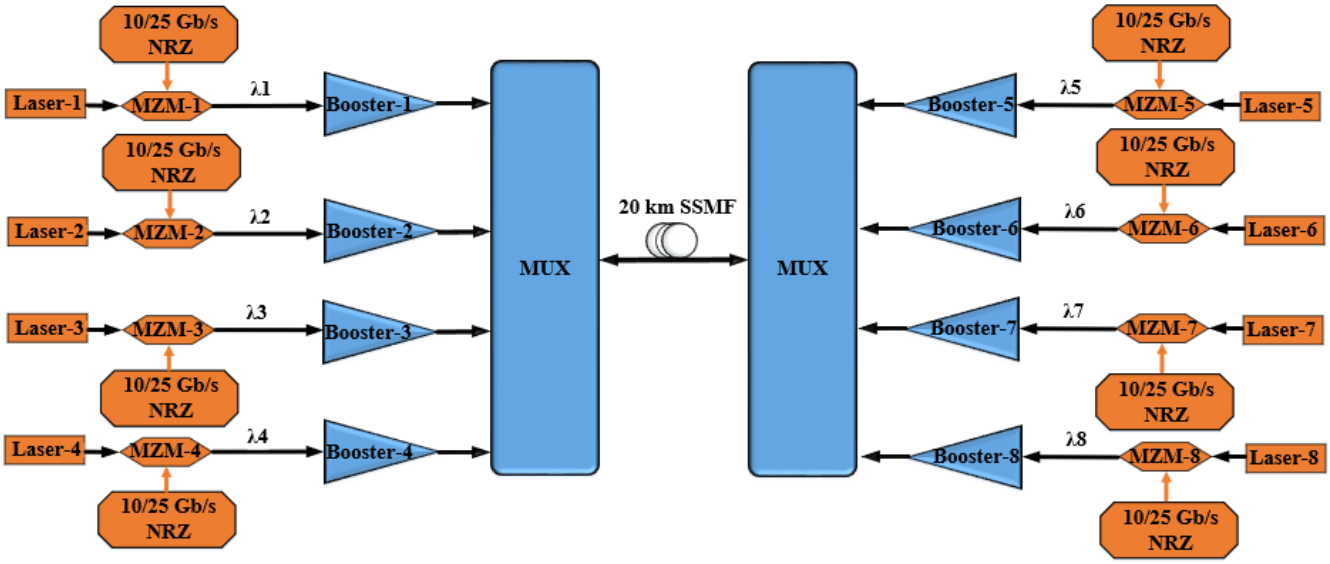

Fig. 3. The simulation setup for investigating the SRS nonlinearity impairment (color online)

Table 3. The used parameters in the simulation

Parameters	Value
Number of Channels	4, 8, 12
Modulation Rate	10 Gb/s, 25 Gb/s
Fiber Attenuation	0.4 dB/km
Dispersion Slope	0.093 ps/nm^2·km
Chirp Coefficient	0
Out Power	6 dBm, 8 dBm, 10 dBm
Fiber Length	10 km, 20 km, 30 km
MUX Insertion Loss	1.5 dB
Zero-dispersion Wavelength	1310 nm

4. Simulation results and analysis

4.1. Effect of bit rate

Firstly, the effect of bit rate on FWM nonlinearity impairment is analyzed, as given in Fig. 4(a). It can be seen that when the bit rate is 10 Gb/s, the obtained sensitivity of Channel 3 after 20 km SSMF transmission is -28 dBm at the case of 1×10^{-2} BER (LDPC-FEC) [26, 27]. However, when Channel 3 is transmitted after Back-to-Back (BtB), the obtained sensitivity is -29 dBm. Therefore, the FWM-induced sensitivity penalty is 1 dB. Similarly, the FWM-induced sensitivity penalty is also 1 dB when the bit rate is increased to 25 Gb/s. Hence, the effect of bit rate on FWM nonlinearity impairment is not apparent.

The impact of bit rate on XPM nonlinearity degradation is next examined and shown in Fig. 4(b). When the bit rate is 10 Gb/s, the achieved sensitivity of Channel 3 after simultaneous transmission is quite similar to that of the single wavelength transmission case. Moreover, when the bit rate is 25 Gb/s, the XPM-induced sensitivity penalty is 0.8 dB in the case of 1×10^{-2} BER. It can be seen that the XPM nonlinearity impairment is closely related to the bit rate, i.e., with the increase of the bit rate, the sensitivity penalty caused by the XPM becomes more severe.

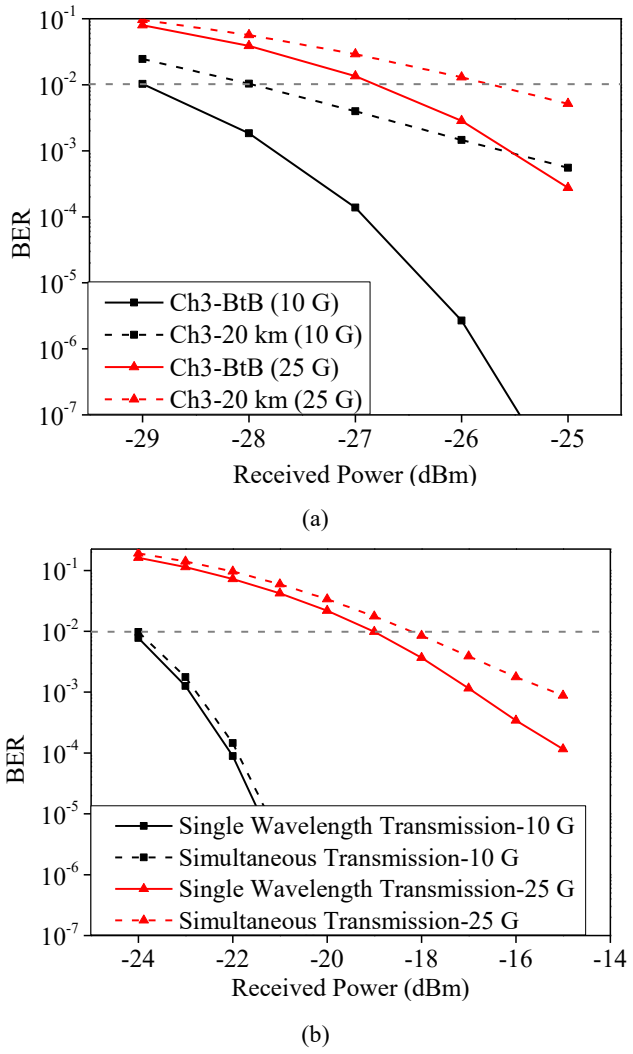

Fig. 4. The measured BER curves for investigating the (a) FWM, (b) XPM nonlinearity impairment when the bit rate is 10 Gb/s and 25 Gb/s (color online)

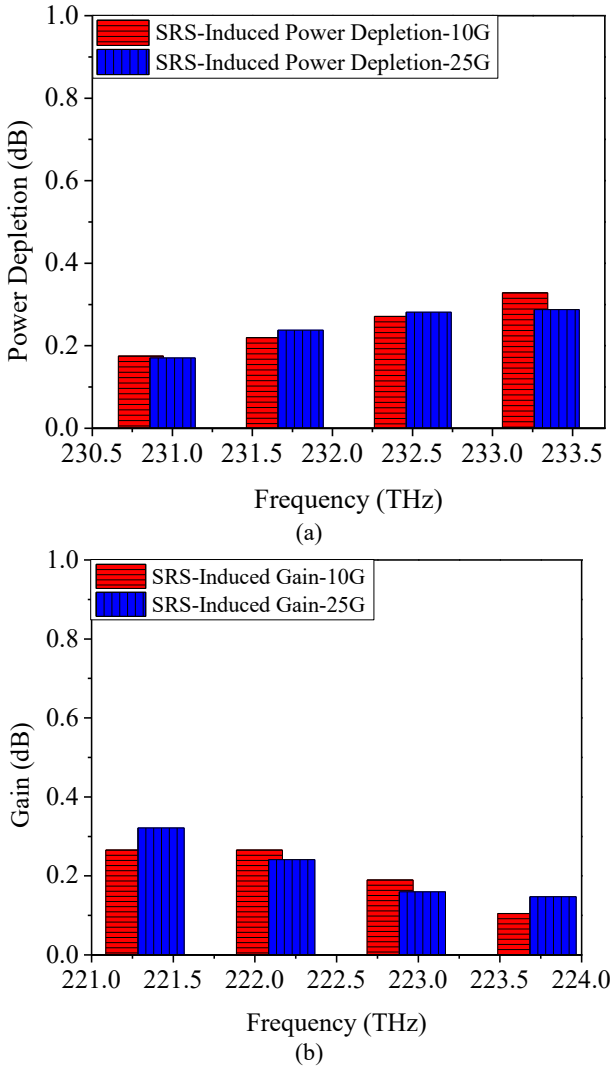

Fig. 5. The SRS-induced optical power changes of the (a) upstream, (b) downstream wavelengths when the bit rate is 10 Gb/s and 25 Gb/s (color online)

Finally, the effect of bit rate on SRS nonlinearity impairment is examined, as shown in Fig. 5. Note that, the SRS-induced power depletion/gain is calculated as the difference of the received optical power after the optical fiber transmission with or without SRS nonlinearity impairment. Fig 5(a) shows the SRS-induced power depletion of the upstream wavelengths (pump channels) when the bit rate is 10 Gb/s and 25 Gb/s, it can be seen that when the frequencies are 231.7 THz and 232.5 THz, the SRS-induced power depletion in the case of 25 Gb/s is larger than that of the 10 Gb/s case. In addition, when the frequencies are 230.9 THz and 233.3 THz, the opposite situation emerges, i.e., the SRS-induced power depletion in the case of 10 Gb/s is larger than that of the 25 Gb/s case. Therefore, it is concluded that the impact of bit rate on SRS nonlinearity impairment is not obvious. Similar results are obtained for the downstream wavelengths (signal wavelengths) as represented in Fig. 5(b). The SRS-induced gain is larger when the frequencies are 221.3 THz and 223.7 THz/222.1 THz and 222.9 THz in the case of 25 Gb/s/10 Gb/s scenario.

4.2. Effect of channel spacing

Here, we analyze the effect of channel spacing on the FWM, XPM, and SRS nonlinearity impairments. Fig. 6(a) shows the achieved BER curves under the condition of different channel spacing. It can be seen that when the channel spacing is 200 GHz, the sensitivity penalty is undeterminable (cannot reach the BER of 1×10^{-2}). However, with the increase of the channel spacing to 400 GHz, the FWM-induced sensitivity penalty is mitigated, which is 1.2 dB. When the channel spacing is 800 GHz, the FWM-induced sensitivity penalty is 1 dB. The FWM nonlinearity impairment gradually decreases with the increase of the channel spacing.

Fig. 6(b) indicates the obtained BER curves of the XPM nonlinearity impairment when the channel spacing is 50 GHz, 100 GHz, and 200 GHz, respectively. Owing to the smaller channel spacing of 50 GHz, the XPM-induced sensitivity penalty is unpredictable for the case of 1×10^{-2} BER. The XPM-induced sensitivity penalty is reduced to

0.8 dB when the channel spacing is increased to 100 GHz. When the channel spacing is increased to 200 GHz, a 0.4-dB sensitivity penalty is acquired. Hence, the XPM nonlinearity impairment is closely related to the channel spacing, i.e., with the increase of the channel spacing, the XPM nonlinearity impairment correspondingly weakens.

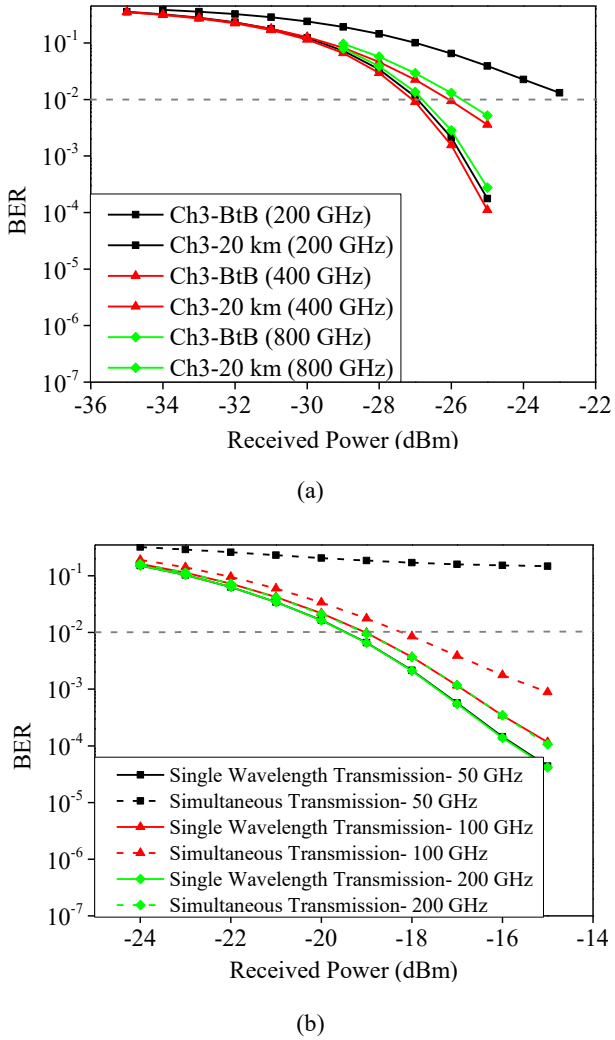

Fig. 6. The measured BER curves for studying the (a) FWM, (b) XPM nonlinearity impairment with different channel spacing (color online)

Fig. 7 illustrates the SRS-induced optical power changes of the upstream and downstream wavelengths when the channel spacing between the upstream and downstream wavelengths is 20 nm, 30 nm, and 40 nm, respectively. From Fig. 7(a), we can see that when the channel spacing is 20 nm, the SRS-induced power depletion is 0.2 dB for the highest frequency. While, with the increase of the channel spacing, the SRS-induced power depletion grows to 0.32 dB (30 nm channel spacing) and 0.35 dB (40 nm channel spacing). Similarly, the SRS-induced gain for the downstream wavelength gradually becomes larger with the increase of the channel spacing, as elucidated in Fig. 7(b).

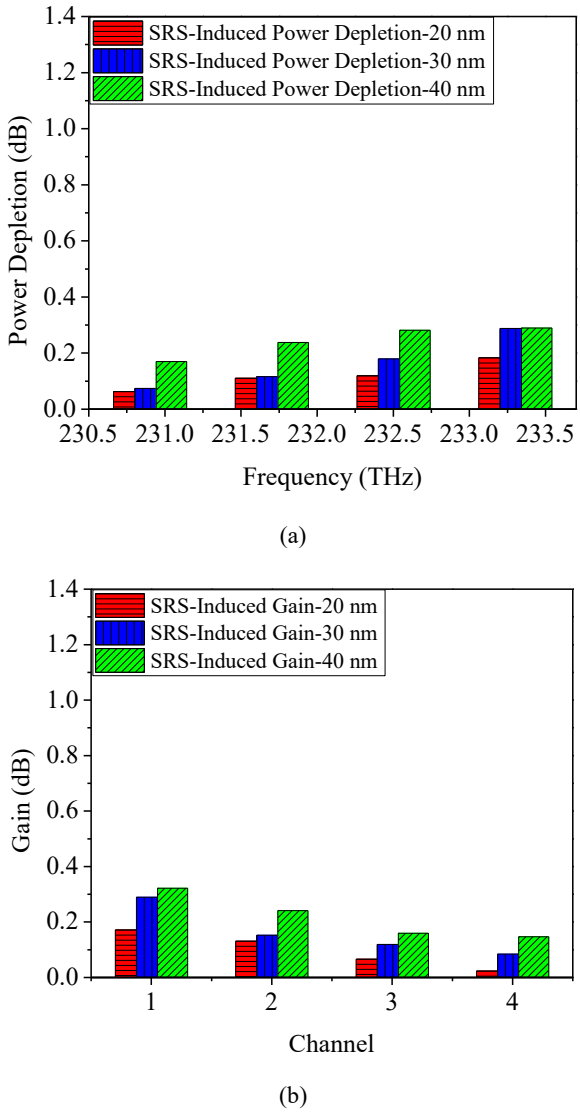

Fig. 7. The SRS-induced optical power changes of the (a) upstream, (b) downstream wavelengths when the channel spacing between the upstream and downstream wavelengths is 20 nm, 30 nm, and 40 nm (color online)

4.3. Effect of chromatic dispersion

In order to further investigate the channel behavior, different chromatic dispersion coefficients are considered in the following section. Fig. 8(a) indicates the BER curves of different chromatic dispersion coefficients effect on the FWM nonlinearity impairment. It can be seen that when the chromatic dispersion coefficient is 0, the FWM nonlinearity impairment is the most severe and causes a 1-dB sensitivity penalty. While, with the increase of the chromatic dispersion coefficient, the FWM nonlinearity impairment becomes negligible (i.e., the BER curves after BtB and 20 km transmission are almost the same) and the FWM-induced sensitivity penalty is close to 0.

Fig. 8(b) shows the BER curves when Channel 3 is considering single wavelength and simultaneous transmission. It can be seen, when the chromatic dispersion coefficient is 3.5 ps/nm/km, the obtained

sensitivity penalty is 0.9 dB at the BER of 1×10^{-2}. When the chromatic dispersion coefficient is 17 ps/nm/km, the achieved sensitivity penalty is 0.8 dB, which is 0.1 dB better than that of the 3.5 ps/nm/km case. The "walk-off" effect between the transmitted channels is made worse by a larger chromatic dispersion coefficient, which mitigates the XPM nonlinearity impairment.

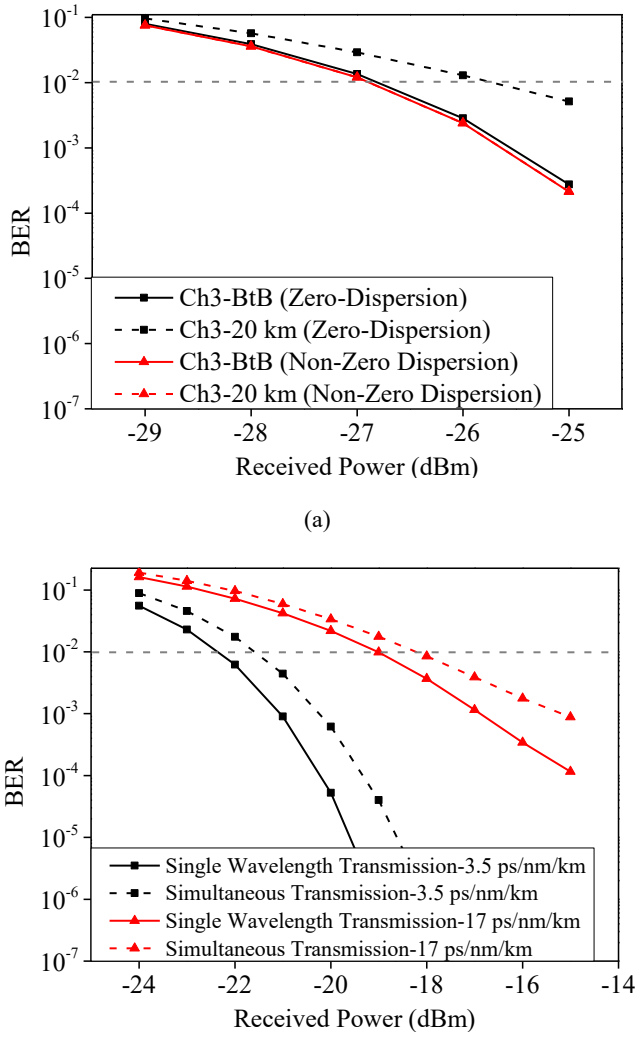

Fig. 8. The measured BER curves for researching the (a) FWM, (b) XPM nonlinearity impairment when the chromatic dispersion coefficient is 3.5 ps/nm/km and 17 ps/nm/km (color online)

Fig. 9 indicates the SRS-induced optical power changes under the condition of different chromatic dispersion coefficients. Here, O-band and C-band upstream and downstream wavelengths are utilized. From Fig. 9(a), it can be seen that when the upstream wavelengths are situated in O-band (lower chromatic dispersion coefficient), the SRS-induced power depletion is 0.3 dB for the highest frequency. While, when the upstream wavelengths are situated in C-band (higher chromatic dispersion coefficient), the SRS-induced power depletion is 0.27 dB for the highest frequency, which is lower than that of the O-band case. Similarly, the SRS-induced gain of the downstream in O-band is larger than that of the C-band scenario. It can be explained that higher chromatic dispersion coefficient leads to the shorter channel-to-channel interactions and thus results in the weakness of the SRS nonlinearity impairment.

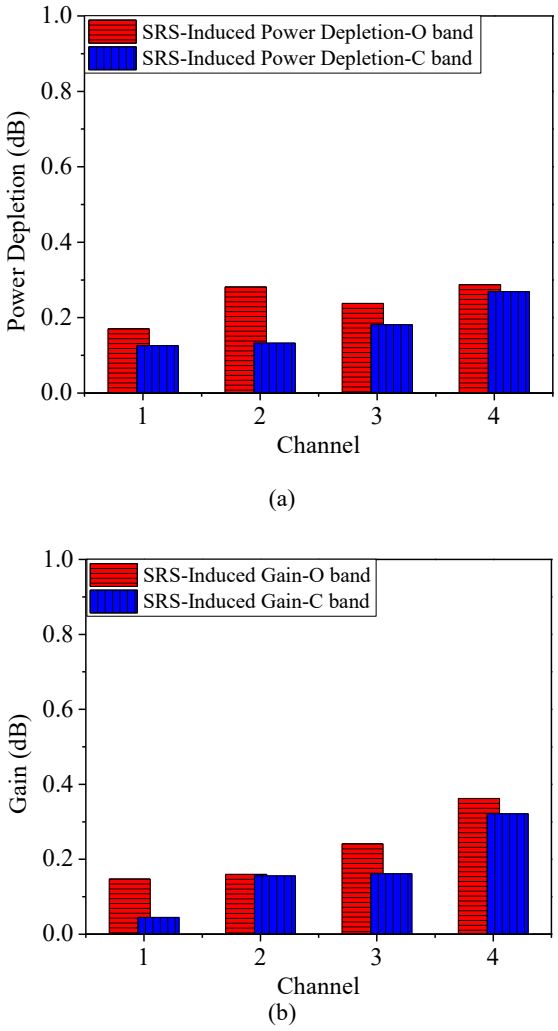

Fig. 9. The SRS-induced optical power changes of the (a) upstream, (b) downstream wavelengths when the upstream and downstream wavelengths are located in O-band and C-band, respectively (color online)

4.4. Effect of fiber length

Fig. 10 illustrates the influence of fiber length on the FWM and XPM nonlinearity impairments. Thereinto, Fig. 10(a) shows the BER curves of the FWM nonlinearity impairment when the fiber length is 10 km, 20 km, and 30 km, respectively. As can be observed, the FWM-induced sensitivity penalty is 0.5 dB for fiber lengths of 10 km. When the fiber length is 20 km, a 1-dB sensitivity penalty is observed due to the FWM nonlinearity impairments. More specifically, the FWM nonlinearity defects cause a 1.4-dB sensitivity penalty when the fiber length approaches 30 km. It can be summarized as follows: longer transmission distance implies longer interaction

times between the transmitted channels, which exacerbates the effects of nonlinearity impairments.

Similarly, the XPM-induced sensitivity penalty grows with the increase of the fiber length as given in Fig. 10(b). The XPM-induced sensitivity penalty is 0.7 dB when the channels transmit over a fiber length of 10 km, whereas the XPM-induced sensitivity penalty is 0.8 dB when the channels transmit over a fiber length of 20 km. Moreover, when the channels are transmitted at 30 km, the XPM-induced sensitivity penalty is impossible to be predicted due to the unreachable of the 1×10^{-2} BER.

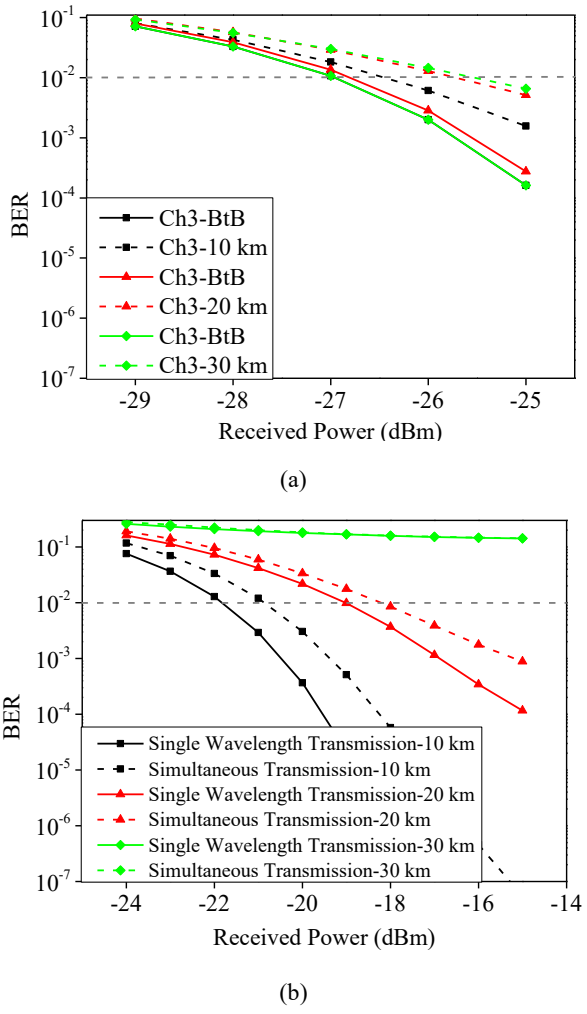

Fig. 10. The measured BER curves for investigating the (a) FWM, (b) XPM nonlinearity impairment when the fiber length is 10 km, 20 km, and 30 km (color online)

Fig. 11 represents the optical power variations caused by SRS nonlinearity impairment when the fiber length is 10 km, 20 km, and 30 km, respectively. Similar to the above-mentioned results of FWM and XPM nonlinearity impairments, with the increase of the fiber length, the SRS-induced optical power variations are increased gradually. From Fig. 11(a), it can be seen that the power depletion increases from 0.3 dB to 0.4 dB when the fiber length extended from 10 km to 30 km. Similar results can be achieved from Fig. 11(b), where the optical power gain increases from 0.25 dB to 0.3 dB with the fiber length increment.

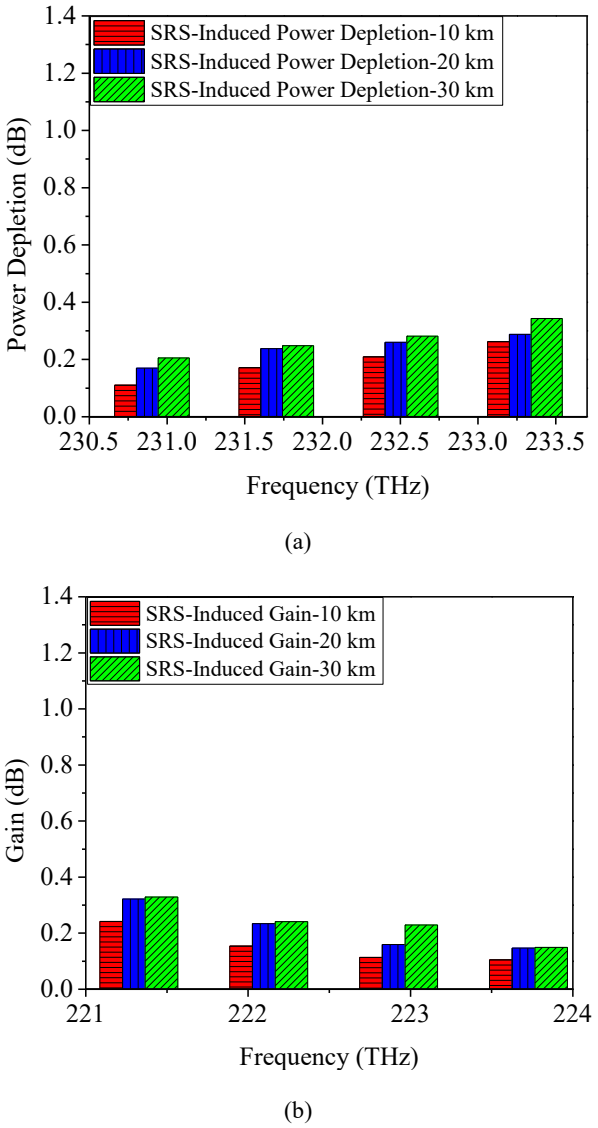

Fig. 11. The SRS-induced optical power changes of the (a)upstream, (b) downstream wavelengths when the fiber (b)length is 10 km, 20 km, and 30 km (color online)

4.5. Effect of input power

Different input powers affect the performance of the FWM, XPM, and SRS nonlinearity impairments, which should be considered. Fig. 12(a) depicts the FWM-induced sensitivity penalty when the input power is 6 dBm, 8 dBm, and 10 dBm per channel. It can be seen that, compared with the 6 dBm case (i.e., 0.4-dB sensitivity penalty is caused by the FWM nonlinearity impairment), when the input power is 8 dBm/10 dBm, the FWM-induced sensitivity penalty is expanded to 1 dB/3.3 dB, which is much more severe than that of the 6 dBm case.

Fig. 12(b) shows the XPM-induced sensitivity penalty when the input power is 6 dBm, 8 dBm, and 10 dBm per channel. We can see that, when the input power is 6 dBm

per channel, the XPM-induced sensitivity penalty is 0.6 dB. However, with the increase of the input power from 8 dBm to 10 dBm, the sensitivity penalty is raised from 0.6 dB to 0.8 dB until 1 dB.

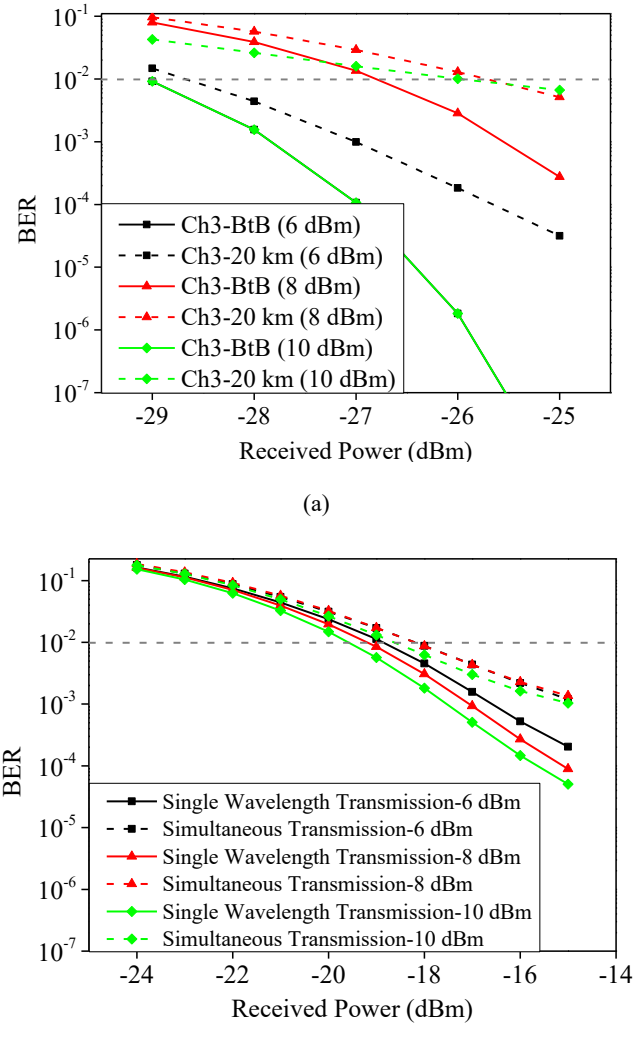

Fig. 12. The measured BER curves for studying the (a) FWM, (b) XPM nonlinearity impairment when the input power is 6 dBm, 8 dBm, and 10 dBm (color online)

In Fig. 13, the SRS-induced optical power changes of the upstream and downstream wavelengths are shown for various input powers, and it can be seen that as the input power rises, so do the power depletion and gain. When the input power is 10 dBm per channel, the power depletion/gain is 0.45 dB/0.32 dB, which is 0.15 dB/0.1 dB larger than that of the 6 dBm case.

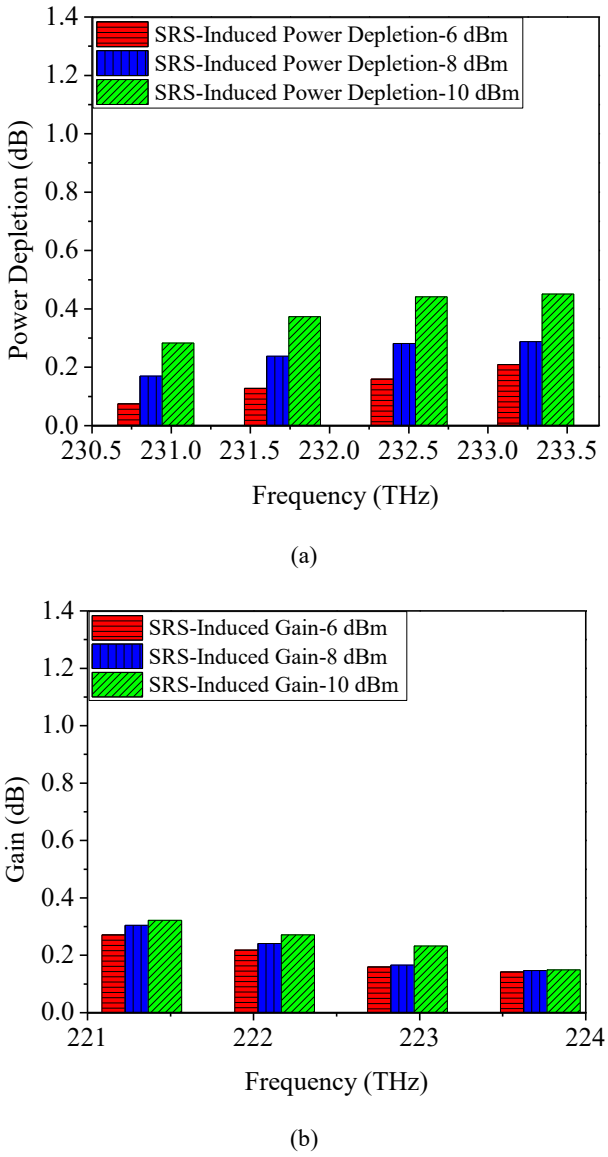

Fig. 13. The SRS-induced optical power changes of the (a)upstream, (b) downstream wavelengths when the input power is 6 dBm, 8 dBm, and 10 dBm (color online)

4.6. Effect of number of channels

In addition, the impact of the number of channels on the FWM, XPM, and SRS nonlinearity impairments is analyzed. Fig. 14(a) depicts the BER curves of the FWM nonlinearity impairment when the number of channels is set as 4, 8, and 12. It can be seen that, with the increase of the number of channels, the FWM-induced sensitivity penalty becomes larger. When the number of channels is 4, a 1-dB sensitivity penalty occurs. When the number of channels is increased to 8, the sensitivity penalty is raised to 3.8 dB. While, when the number of channels is 12, unpredictable sensitivity penalty is acquired due to the most severe FWM nonlinearity impairment.

Fig. 14(b) elucidates the BER curves of the XPM nonlinearity impairment under different number of channels. It can be seen that when the number of channels

is 4, 8, and 12, the XPM-induced sensitivity penalty is nearly the same, which is 0.8 dB. Although the number of channels is increased in the system, the influence of the distant channels on the target channel can be ignored owing to the "walk-off" effect. While, the effect of the XPM nonlinearity impairment on the whole system becomes exceedingly severe due to the number of channels increment.

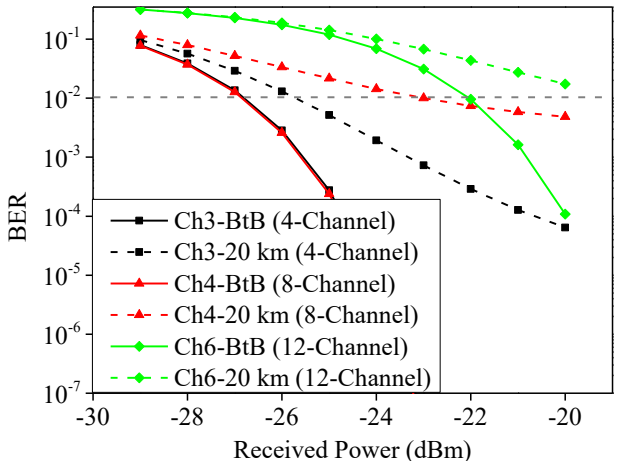

(a)

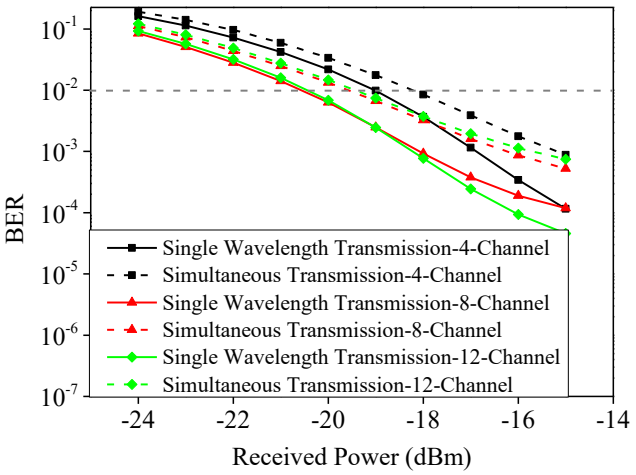

(b)

Fig. 14. The measured BER curves for investigating the (a) FWM, (b) XPM nonlinearity impairment when the number of channels is 4, 8, and 12 (color online)

Fig. 15 represents the SRS-induced optical power changes of the upstream and downstream wavelengths under the circumstance of 4, 8, and 12-channel system. Similar to the above-mentioned FWM results, with the increase of the number of channels, the power depletion/gain caused by the SRS nonlinearity impairment becomes larger. It can be explained that more channels participate in the nonlinearity impairment process, leading to the more severe SRS and larger optical power changes.

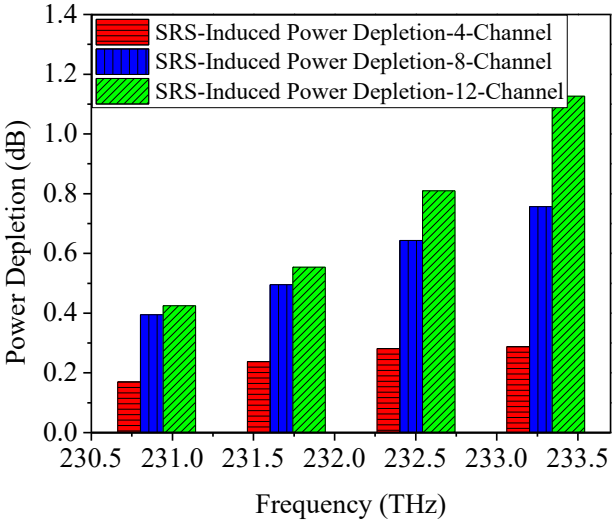

(a)

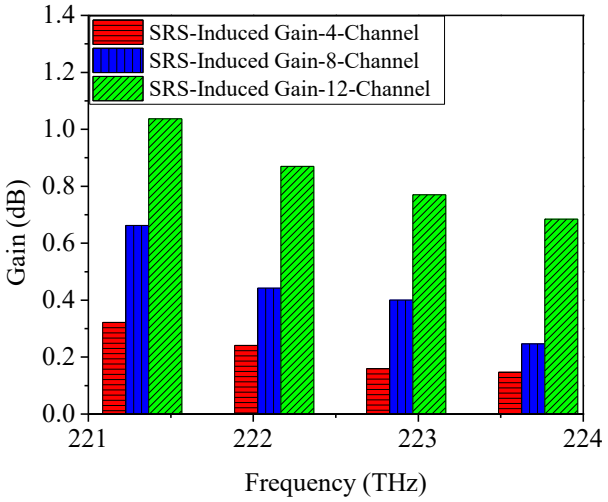

(b)

Fig. 15. The SRS-induced optical power changes of the (a) upstream, (b) downstream wavelengths when the number of channels is 4, 8, and 12 (color online)

4.7. Effect of dark current

Fig. 16 shows the acquired BER curves when the dark current parameter is selected as the variate. Thereinto, Fig. 16(a) gives the obtained results when Channel 3 suffers the FWM nonlinearity impairment under different dark currents. It is observed that, with a BER threshold value of 1×10^{-2}, the BER curves overlap following BtB and 20-km optical fiber transmission, regardless of whether the dark current is 1E-8, 2E-8, or 3E-8 A. This suggests that variations in dark current do not significantly impact the impairment caused by FWM nonlinearity. Similar results are obtained when Channel 3 suffers the XPM nonlinearity impairment, which can be seen in Fig. 16(b).

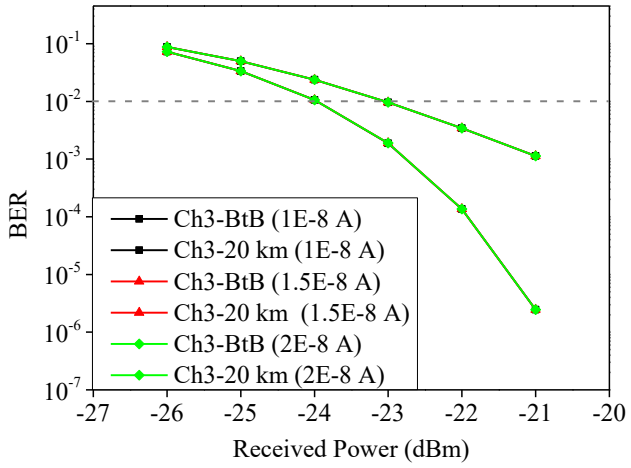

(a)

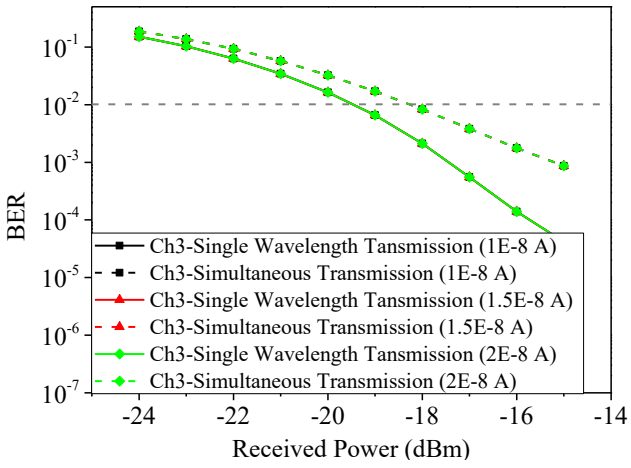

(b)

Fig. 16. The measured BER curves for investigating the (a) FWM, (b) XPM nonlinearity impairment when the dark current is 1E-8, 1.5E-8 and 2E-8 A (color online)

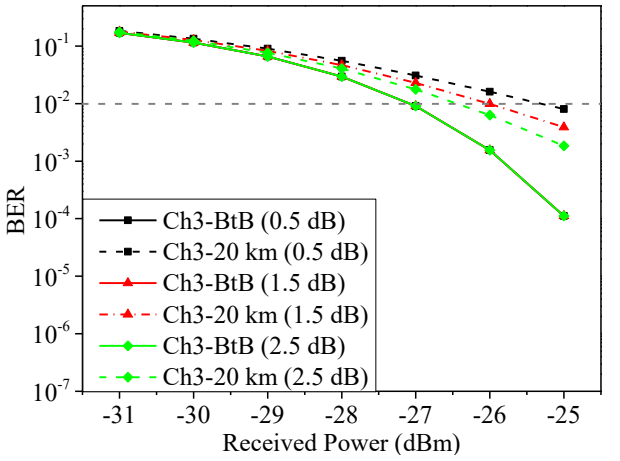

(a)

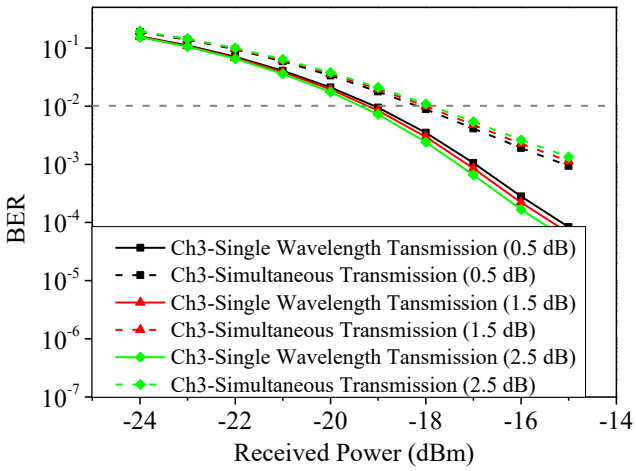

(b)

Fig. 17. The measured BER curves for investigating the (a) FWM, (b) XPM nonlinearity impairment when the insertion loss is 0.5, 1.5 and 2.5 dB (color online)

4.8. Effect of insertion loss

Regarding the parameter of insertion loss, the obtained results are represented in Fig. 17. From Fig. 17(a), we can see that when the insertion loss is 0.5 dB, the FWM-induced sensitivity penalty is 1.6 dB. While, with the increase of insertion loss to 1.5 dB, the measured sensitivity penalty is decreased to 1 dB. Better still, when the insertion loss is set as 2.5 dB, the sensitivity penalty is 0.5 dB, which is 1.1 dB better than that of the 0.5-dB insertion loss case. It can be explained that higher insertion loss means lower input power, and under the condition of lower input power, the effect of nonlinearity impairment on the transmitted wavelengths is reduced correspondingly. Similar results can be obtained when Channel 3 is affected by XPM, as given in Fig. 17(b). It can be seen that, with the increase of the insertion loss, the XPM-induced sensitivity penalty gradually improved.

4.9. Effect of dispersion slope

Here, we discuss the effect of dispersion slope on FWM and XPM nonlinearity impairment, which is illustrated in Fig. 18. It can be see that, similar to the obtained conclusion above-mentioned when dark current is selected as the variate, the FWM and XPM-induced sensitivity penalty on Channel 3 does not change under different dispersion slopes, i.e., changing dispersion slope has negligible effect on FWM and XPM nonlinearity impairment.

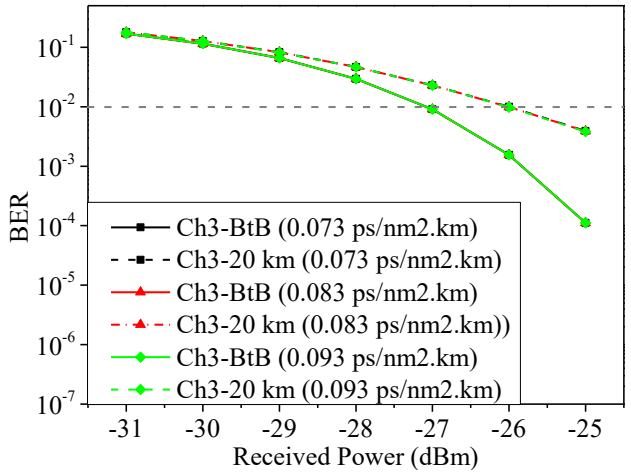

(a)

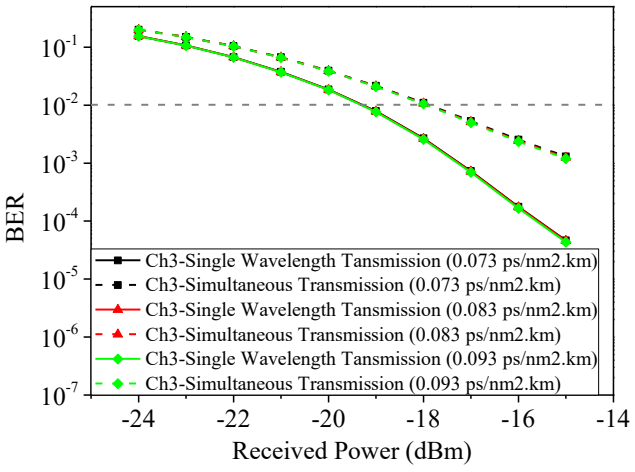

(b)

Fig. 18. The measured BER curves for investigating the (a) FWM, (b) XPM nonlinearity impairment when the dispersion slope is 0.073, 0.083 and 0.093 ps/nm^2·km (color online)

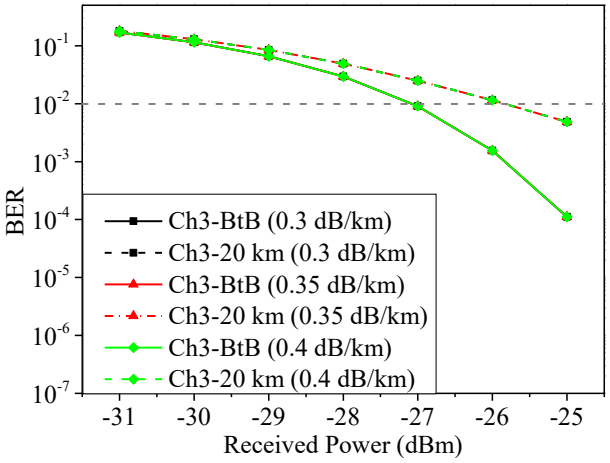

(a)

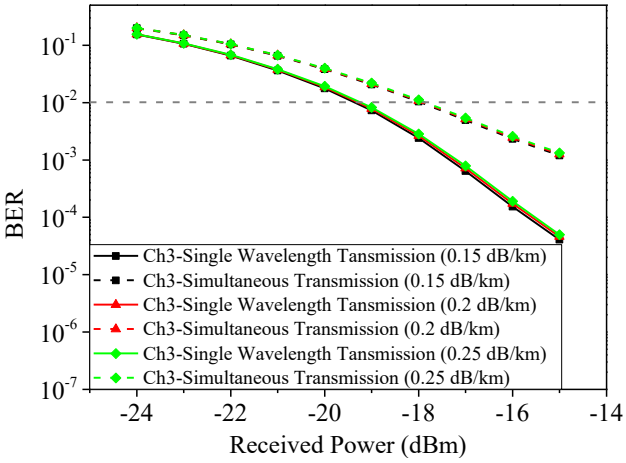

(b)

Fig. 19. The measured BER curves for investigating the (a) FWM, (b) XPM nonlinearity impairment when the fiber attenuation is 0.3, 0.35 and 0.4 dB/km for O-band and 0.15, 0.2 and 0.25 dB/km for C-band (color online)

4.10. Effect of fiber attenuation

Afterwards, the FWM and XPM-induced sensitivity penalty under different fiber attenuation values are given in Fig. 19. Considering the distinct fiber attenuation characteristics of the O-band and C-band, fiber attenuation values of 0.3, 0.35, and 0.4 dB/km have been chosen for O-band transmission, while 0.15, 0.2, and 0.25 dB/km have been selected for C-band transmission. However, regardless of changes in fiber attenuation values, the sensitivity penalty resulting from FWM and XPM remains unaffected, indicating that the impact of fiber attenuation on FWM is minimal.

4.11. Effect of chirp coefficient

Finally, the FWM and XPM-induced sensitivity penalty under different chirp coefficients are investigated. As shown in Fig. 20 (a), there is no change in the FWM-induced sensitivity penalty on Channel 3 after BtB and 20-km optical fiber transmission, even as the chirp coefficient increases from 0 to 1. This indicates that FWM nonlinearity impairment is insensitive to variations in the chirp coefficient. This insensitivity arises because Channel 3 is configured at the zero-dispersion wavelength to maximize the impact of FWM nonlinearity impairment. Consequently, in the absence of chromatic dispersion's influence, the chirp coefficient's effect on the BER is minimal. In contrast, as depicted in Fig. 20 (b), it is observed that with a chirp coefficient of 0, the sensitivity penalty induced by XPM is 1 dB. However, with the chirp coefficient increased to 0.5, the BER curves deteriorate to the extent that they fail to meet the 1×10^{-2} BER threshold,

leading to an unpredictable sensitivity penalty. A similar outcome is observed when the chirp coefficient is adjusted to 1. This can be attributed to the C-band being significantly affected by chromatic dispersion, which, when combined with the chirp coefficient, exacerbates the BER deterioration.

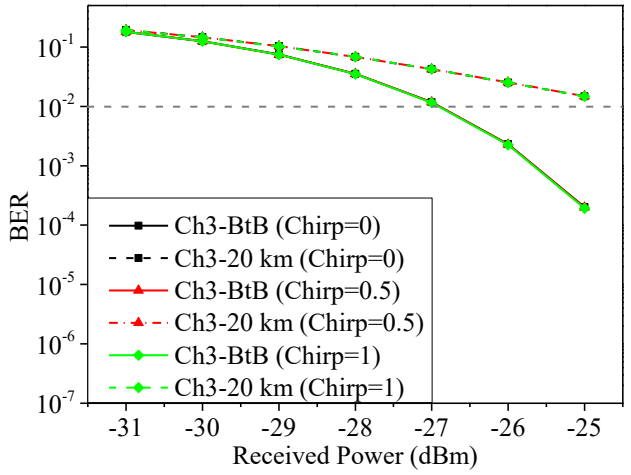

(a)

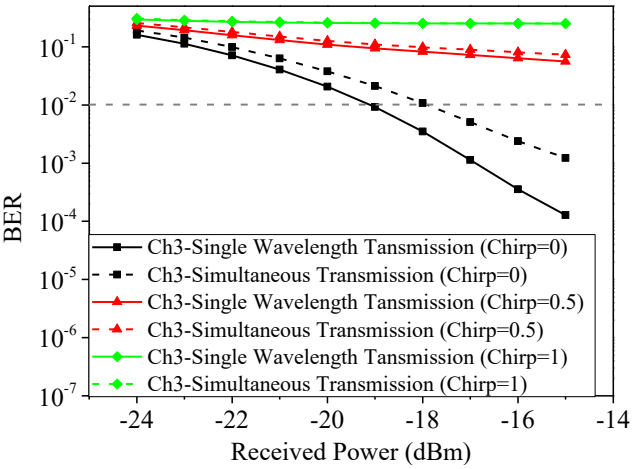

(b)

Fig. 20. The measured BER curves for studying the (a) FWM, (b) XPM nonlinearity impairment with different chirp coefficients (color online)

5 Conclusions

In this paper, the effect of different parameters, including the bit rate, channel spacing, chromatic dispersion, fiber length, input power, number of channels, dark current, insertion loss, dispersion slope, fiber attenuation and chirp coefficient on the FWM, XPM, and SRS nonlinearity impairments are analyzed sufficiently through theory and simulation. Besides, the effects of fiber nonlinearity on sensitivity penalty and optical power variations under various parameters are presented in detail. Based on the simulation results, it has been determined that a number of parameters should be taken into account to mitigate the FWM, XPM, and SRS nonlinearity impairments. Since the proposed simulation systems account for the scalability and future-proofing of WDM-based PON networks, the results presented can serve as valuable references for the development of WDM-based PON networks that achieve the intended performance.

Disclosures

The authors declare that there are no conflicts of interest regarding the publication of this paper.

Code, Data, and Materials Availability

The manuscript does not have associated code, supporting data and required data availability statement.

References

[1] CISCO, “Cisco Visual Networking Index: Forecast and Trends, 2017-2022,” https://www.cisco.com/c/en/us/solutions/service-provider/index.html.
[2] A. Saleem, H. Cui, Y. He, A. Boag, IEEE Antenn. Propag. M. **64**(3), 126 (2022).
[3] J. Montalvo, J. Torrijos, D. Cortes, Proceedings of 2020 European Conference on Optical Communications (ECOC), 6-10 December, 2020.
[4] A. Saleem, Y. Xu, R. Khan, I. Rasheed, Z. Jaffri, M. Layek, Wirel. Commun. Mob. Com. **22**, 9090494 (2022).
[5] Y. Song, P. Yu, Y. Xu, Z. Li, Opt. Fiber Technol. **65**, 102628 (2021).
[6] F. Ali, F. Muhammad, U. Habib, Y. Khan, M. Usman, Photonic Netw. Commun. **41**, 36 (2021).
[7] G. Agarawal, “Nonlinear Fiber Optics,” 3rd edition, Academic Press 2001.
[8] F. Ali, Y. Khan, A. Ali, G. Ahmad, J. Opt. Commun. **42**(2), 289 (2018).
[9] X. Miao, M. Bi, H. He, W. Hu, Proceedings of 2017 Opto-Electronics and Communications Conference (OECC) and Photonics Global Conference (PGC), July 31-August 4, 2017.
[10] X. Wu, Z. Li, Y. Song, Y. Guo, Y. Yin, M. Wang, Opt. Commun. **403**, 335 (2017).
[11] R. Oliveira, E. Silva, U. Costa, R. Ferreira, A. Shahpari, J. Costa, A. Teixeira, Proceedings of 2017 19th International Conference on Transparent Optical Networks (ICTON), July 2-6, 2017.
[12] M. Abdulnabi, W. Saad, B. Hamza, Journal of Physics: Conference Series **1530**, 012158 (2020).
[13] R. Pagare, S. Kumar, A. Mishra, Journal of Optical Communications **44**(s1), s0299 (2021).
[14] R. Gaudino, V. Curri, S. Capriata, Proceedings of 2013 European Conference and Exhibition on Optical Communication (ECOC), September 22-26, 2013.

[15] V. Curri, S. Capriata, R. Gaudino, Proceedings of 2014 Optical Fiber Communications Conference (OFC*)*, March 9-13, 2014.
[16] G. Simon, F. Saliou, P. Chanclou, B. Guyader, L. Guillo, Proceedings of 2015 Optical Fiber Communications Conference (OFC), March 22-26, 2015.
[17] Y. Xu, P. Yu, N. Ye, Y. Song, Opt. Eng. **59**(7), 076114 (2020).
[18] M. Wu, W. Way, J. Lightwave Technol. **22**(6), 1483 (2004).
[19] Y. Xu, P. Yu, N. Ye, Q. Zhang, Y. Song, Opt. Fiber Technol. **67**, 102727 (2021).
[20] J. Li, H. He, W. Hu, Opt. Express **23**(7), 8809 (2015).
[21] K. Hinzer, T. Hall, J. Mod. Opt. **66**(3), 287 (2019).
[22] M. Irfan, F. Ali, F. Muhammad, U. Habib, A. Alwadie, A. Glowacz, Z. Abbas, E. Kańtoch, Entropy **22**(9), 1062 (2020).
[23] F. Muhammad, F. Ali, G. Abbas, Z. Abbas, S. Haider, M. Bilal, M. Piran, D. Suh, Electronics **10**(5), 611 (2021).
[24] F. Ali, M. Shakeel, A. Ali, W. Shah, M. Qamar, S. Ahmad, U. Ali, M. Waqas, J. Opt. Commun. **44**(s1), s1225 (2023).
[25] Sumitomo Electric Device Innovation, INC. http://www.sedi.co.jp/data.jsp?version=en&database=opticaldevices&id=316&class=03012208.
[26] D. Lu, Y. Zhao, H. He, Y. Rao, H. Shi, S. Huang, H. Yu, Z. Dong, J. Mod. Opt. **69**(12), 693 (2022).
[27] M. Li, V. Derudder, K. Bertrand, C. Desset, A. Bourdoux, IEEE Transactions on Circuits and Systems I **68**(5), 2224 (2021).

*Corresponding author: 840181531@qq.com; Beryly@shu.edu.cn